Chapter 4

Effect of Photoluminescent Carbon Dots on the Efficiency of Dye Sensitized Solar Cell with Poly(methyl methacrylate) Based Polymer Gel Electrolyte

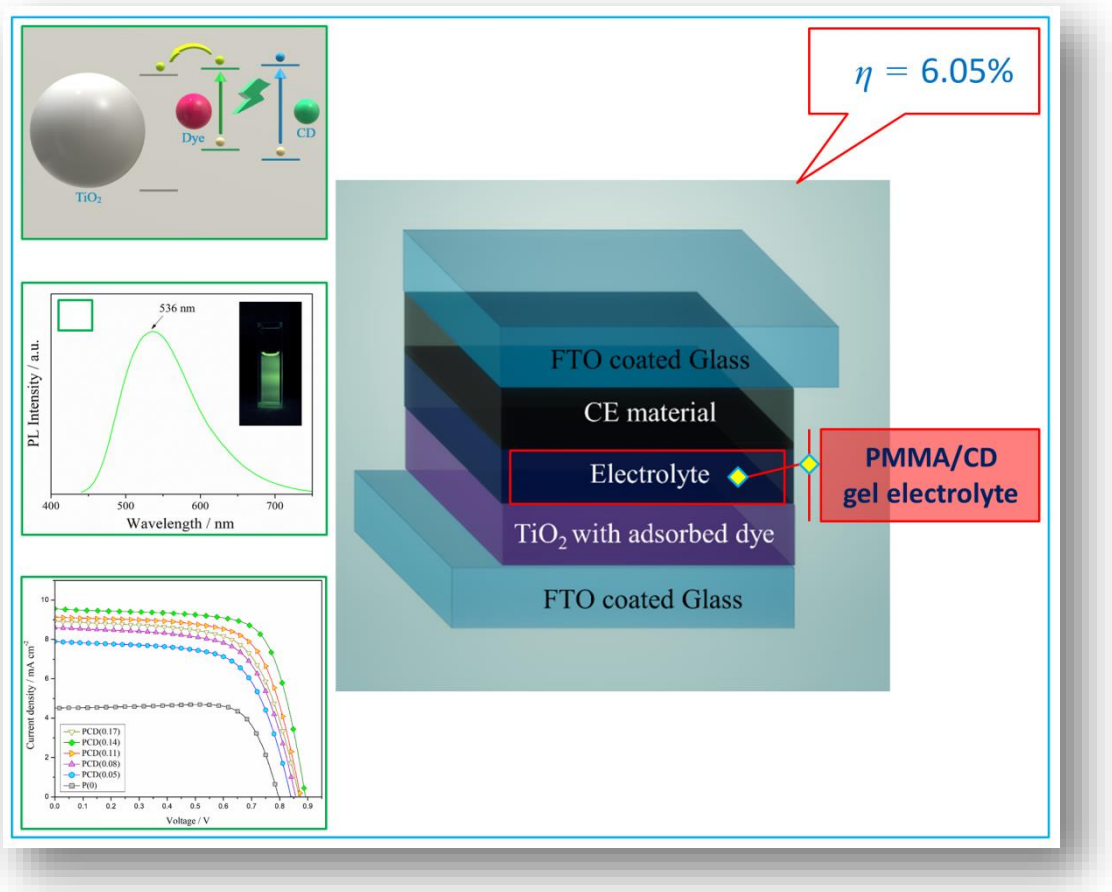

DSSC based on CD modified PGE utilizes the unused higher energy visible light to give an enhanced efficiency of 6.05%.

4.1 Introduction

Herein, we report an efficient and durable dye sensitized solar cell (DSSC) fabricated with polymer gel electrolyte (PGE) based on poly(methyl methacrylate) (PMMA) and green emitting carbon dots (CDs). The optimized DSSC fabricated using the PGE with 0.14 w/v% of CDs in PMMA exhibits a photoconversion efficiency of 6.05 % having open-circuit voltage (V_{OC}) of 0.892 V, short-circuit current density (J_{SC}) of 9.55 mA cm^{-2} and fill factor (*FF*) of 0.70. Moreover, the fabricated DSSC shows significant long-term stability.

DSSCs face major limitation that they can convert only a portion of the sunlight into electrical energy by absorbing light of certain wavelengths. Nonetheless, some part of the unexploited solar light can be additionally harvested by using a specific fluorophore. Yun et al. reported a DSSC with a florescent gel electrolyte of 4-(dicyanomethylene)-2-methyl-6-(4-dimethylaminostyryl)-4H-pyran which showed 1.8 times better performance compared to the DSSC without the fluorescent material [1]. Yao et al. introduced some rare earth ions doped with various host materials which exhibited upconversion and downconversion with required wavelengths of light [2]. Many fluorophores and fluorescent nanoparticles are used in DSSCs to broaden the sunlight absorption region [3,4]. Amongst them, carbon dots (CDs) are of our prime interest because they can emit the required wavelength to excite electrons in dye molecules by absorbing unused lower wavelength of sunlight. Since the dye molecules absorb green light, CDs with green fluorescence have the potential to enhance the efficiency of the DSSCs. However, reports of green emitting CDs are fewer as compared to that of blue emitting ones [5,6]. Moreover, durability is a grave issue faced by DSSCs because of the high volatility and leakage caused by the organic solvents used in the electrolyte. Introducing a polymer in the liquid electrolyte (polymer gel electrolyte, PGE) has been shown to appreciably increase its long-term stability [7–10].

This part of the thesis is published in:

Mohan, K., Bora, A., and Dolui, S. K. Efficient Way of Enhancing the Efficiency of a Quasi-Solid-State Dye-Sensitized Solar Cell by Harvesting the Unused Higher Energy Visible Light Using Carbon Dots. *ACS Sustainable Chemistry & Engineering*, 6(8):10914-10922, 2018.

4.2 Experimental Section

4.2.1 Materials

Diammonium hydrogen citrate and urea were bought from Aldrich. All the other materials used for the experiments were same as mentioned in Section 2.2.1 of Chapter 2.

4.2.2 Synthesis of CDs

The green emitting CDs were prepared by a facile solid state reaction of diamonium hydrogen citrate and urea. 0.2 g each of diammonium hydrogen citrate and urea were mixed and thoroughly grinded in an agate mortar. The mixture was then subjected to 180 °C for an hour in a muffle furnace to obtain the product which was subsequently dissolved in double distilled water. To separate the larger particles, the dispersion was first centrifuged at 12000 rpm for 5 min and then filtered using a 0.22 μm nitrocellulose membrane. The solvent was removed using rotary evaporator to get CDs in powder form. The final product was stored in a desiccator for further use [11].

4.2.3 Preparation of the polymer gel electrolytes

The PGEs were prepared by dispersing PMMA with different amount of CDs in the liquid electrolyte. The polymer matrix, PMMA, was prepared by free radical polymerization of methyl methacrylate initiated by benzoyl peroxide. The PGE with 0.05, 0.08, 0.11, 0.14 and 0.17 w/v % of CDs with respect to the liquid electrolyte are symbolized as PCD(0.05), PCD(0.08), PCD(0.11), PCD(0.14) and PCD(0.17) for better presentation. PGE without CD is denoted as P(0). Iodine (0.05 M), 1-methyl 3-propylimidazolium iodide (0.06 M), lithium iodide (0.5 M) and t-butyl pyridine (0.5 M) were mixed in a 2:8 solvent mixture of N-methyl 2-pyrrolidone (NMP) and acetonitrile to prepare the liquid electrolyte [12,13].

4.2.4 Device fabrication

To prepare the photoanode, clean fluorine doped tin oxide (FTO) coated glass sheets were treated with titanium tetrachloride ($TiCl_4$) solution. A paste of titanium dioxide (TiO_2) prepared in ethanol was deposited on the $TiCl_4$ treated FTO glass *via* doctoral blade method. Subsequently, the film was dipped in N719 dye solution to obtain the photoanode. To fabricate the platinum (Pt) counter electrode, chloroplatinic acid (H_2PtCl_6) was spin coated onto a clean FTO glass and reduced with sodium borohydride ($NaBH_4$). The detailed electrode preparation techniques are given in Section 2.2.5 of Chapter 2. The prepared PCD gel electrolytes were sandwiched between the two electrodes using Solaronix thermal polymer spacers (thickness = 25 μm) to fabricate the DSSCs. Next, the devices were kept at 60°C for 5 min. The temperature aids

in improving the contact between the PCD gel electrolyte and the surface of the electrodes [14,15].

4.2.5 Characterization

The transmission electron microscope (TEM) image and particle size distribution of the prepared CDs were obtained on a Tecnai G2 20 S-TWIN (200kV) instrument and Nanotrac Wave instrument respectively. X-ray photoelectron spectroscopy (XPS) plots of the CDs were recorded using a Kratos Axis-Ultra spectrometer. The structural properties of the materials were characterized using Fourier transform infrared (FTIR) spectroscopy. For studying the absorbance properties of CDs, N719 dye molecules and PMMA/CD composites, ultraviolet-visible (UV-vis) spectroscopy was used. Photoluminescence (PL) spectra of the samples were recorded using a Hitachi F-2700 Fluorescence spectrophotometer. The photovoltaic performance of the DSSCs was analyzed from their current density-voltage (*J-V*) characteristics recorded under irradiation. The electrochemical impedance spectroscopy (EIS) data was recorded under irradiation of light in the frequency range of 0.1 Hz - 1MHz at 10 mV amplitude. The chemical capacitance ($C\mu$) at the photoanode/electrolyte interface was also calculated using EIS plot.

4.3 Results and Discussion

4.3.1 Characterization of CDs

4.3.1.1 Morphology and particle size distribution of CDs

The morphology of the prepared CDs was characterized by using TEM (**Figure 4.1(a)**). From the TEM micrograph, the monodispersity of the CDs is quite evident and the particles scatter in a regular manner. The high resolution TEM (HRTEM) micrograph of CDs (inset of **Figure 4.1(a))** reveals the structure of the CDs as being crystalline. **Figure 4.1(b)** displays the particle size distribution obtained by dynamic light scattering (DLS). The CD particles possess an average size of 4.5 nm with a narrow size distribution (2 to 7 nm). The lattice spacing is 0.21 nm corresponding to the (100) graphitic plane [16].

4.3.1.2 Structural analyses

Figure 4.2 exhibits the FTIR spectra of CD, PMMA and PMMA/CD respectively. In the FTIR spectra of CD, the broad band from 3484 cm^{-1} to 3178 cm^{-1} is ascribed to –OH/–NH stretching vibrations. The peaks at 1708 cm^{-1} and 1597 cm^{-1} are due to O–C=O and C=C stretching vibrations respectively. The peak at 1159 cm^{-1} represents the characteristic stretching vibration of the amine N–H bond. In case of PMMA, the peaks at around 2953 cm^{-1} and 1453

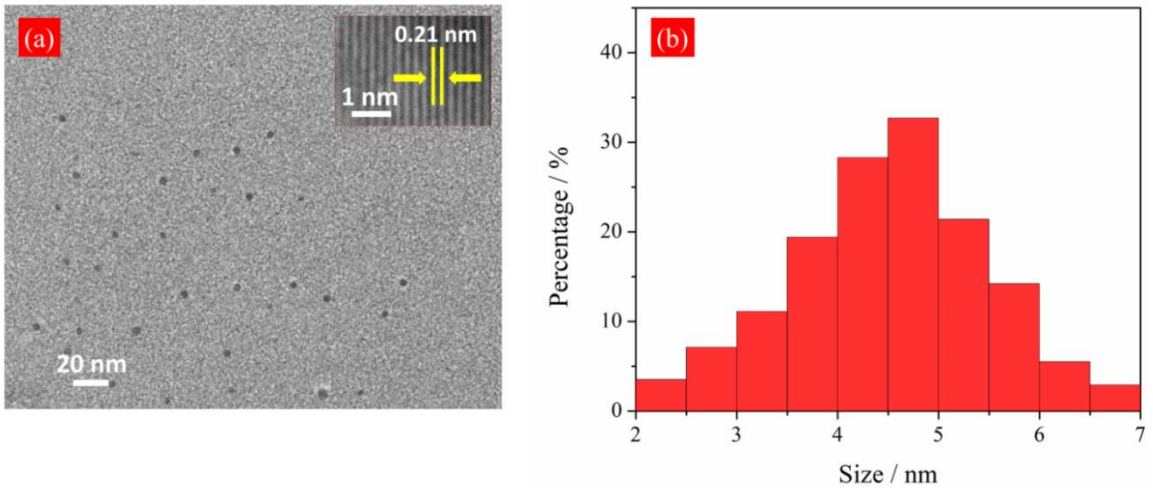

Figure 4.1. (a) TEM and (inset) HRTEM micrographs, and **(b)** particle size distribution of CDs.

cm^{-1} are observed due to the stretching and bending vibrations of C-H bond respectively. A peak at 1734 cm^{-1} and peaks at around 1145 cm^{-1} are observed because of the stretching vibrations of C-O and C=O bonds present in the ester group respectively. The polar nature of the functional groups present in PMMA play an important role in the formation of gel electrolytes. The peak at 987 cm^{-1} is ascribed to the characteristic peak of PMMA. A broad peak at around 3442 cm^{-1} is observed because of the vibration of O-H bond of water molecule adsorbed on the PMMA matrix. PMMA/CD exhibits the characteristic peaks of both the constituting ingredients (CD and PMMA), affirming the successful formation of the composite.

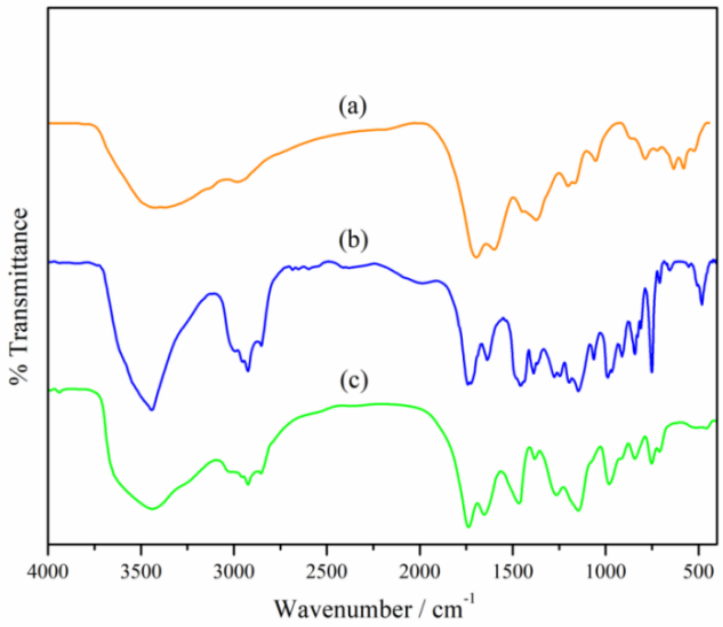

Figure 4.2. FTIR spectra of **(a)** CD, **(b)** PMMA and **(c)** PMMA/CD.

The XPS pattern of C1s band can be deconvoluted into three peaks (**Figure 4.3(a)**). The peaks at 288.1 eV, 286.1 eV and 284.6 eV are ascribed to carboxyl carbon (O–C=O), sp^3 carbon (C–O/C–N) and sp^3/sp^2 carbon (C-C/C=C) respectively. Three deconvoluted peaks in **Figure 4.3(b)** at 400.6 eV, 399.5 eV and 398.8 eV correspond to C_3–N, amino N (N–H) and C–N–C for N1s respectively. **Figure 4.3(c)** exhibits the O1s band which contains two peaks at 532.2 eV and 531.3 eV credited to sp^3 (C–O) and sp^2 (C=O) of the CDs [11].

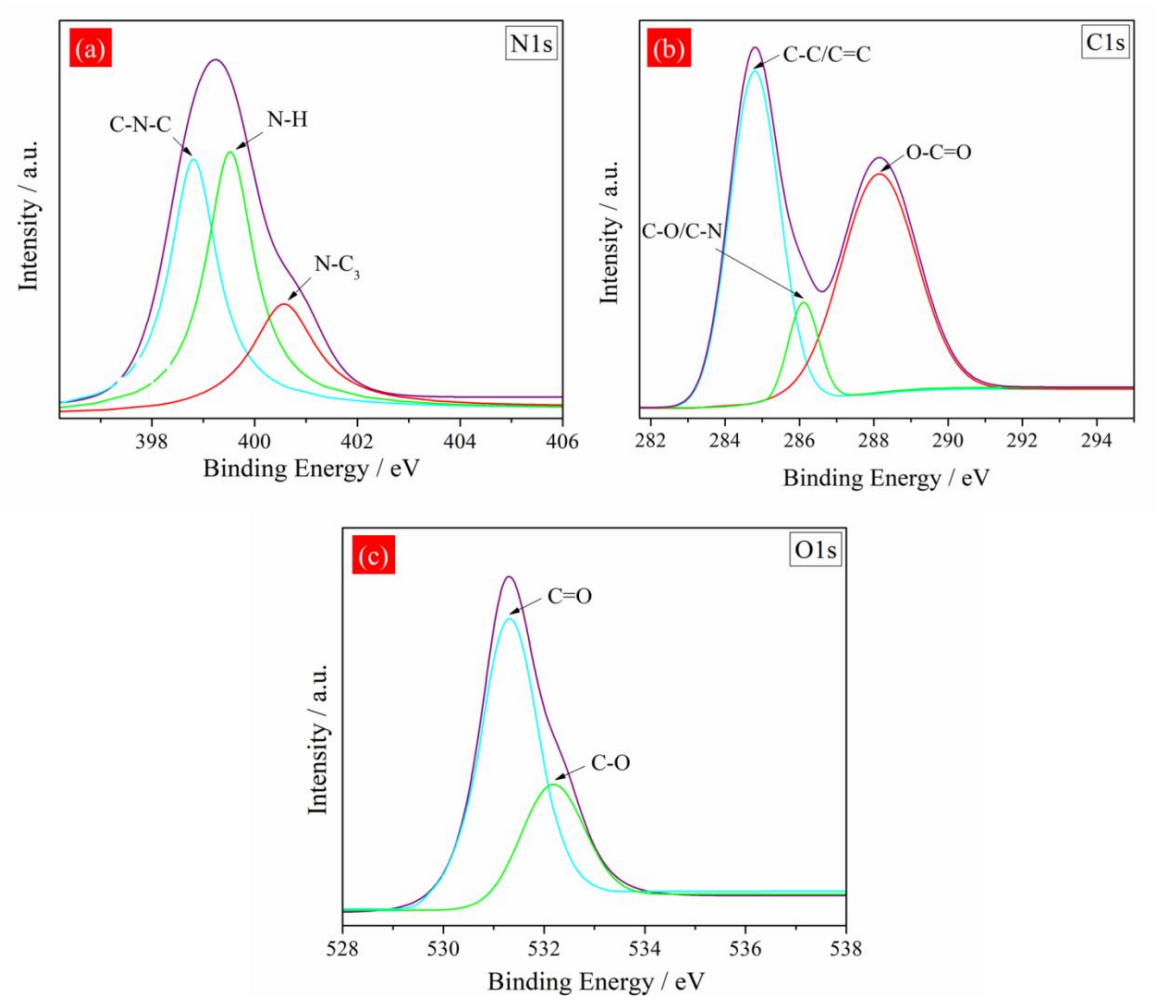

Figure 4.3. Deconvoluted XPS curves of the green emitting CDs.

4.3.2 Optical properties of the materials

4.3.2.1 Optical properties of CDs

A solvent mixture of NMP and acetonitrile (2:8 volume ratio) was used to prepare the electrolyte for DSSC. Consequently, 0.14 w/v % of CDs was dispersed ultrasonically in the acetonitrile and NMP solvent mixture (8:2) to examine their optical properties. Two absorption peaks appear in the UV-vis spectrum at 274 and 410 nm due to the carbonic core center and the

surface or molecular center of the CDs (**Figure 4.4**) [17]. CDs consist of different oxygen containing functional groups as evidenced from the XPS analysis and FTIR spectra. These functional groups form "*surface states*" in the CDs and their energy levels lie between the π and π* states. The absorption at 274 nm is ascribed to the energy difference between the π and π* states of carbonic/aromatic core of the CDs. Additionally, the excitation of electrons from the energy level of surface states (n) to the π* state of the carbonic core of CDs gives rise to another absorption peak at around 420 nm.

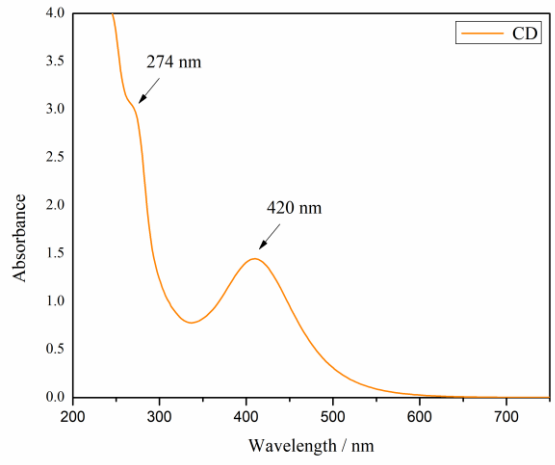

Figure 4.4. UV-vis absorption spectrum of CDs.

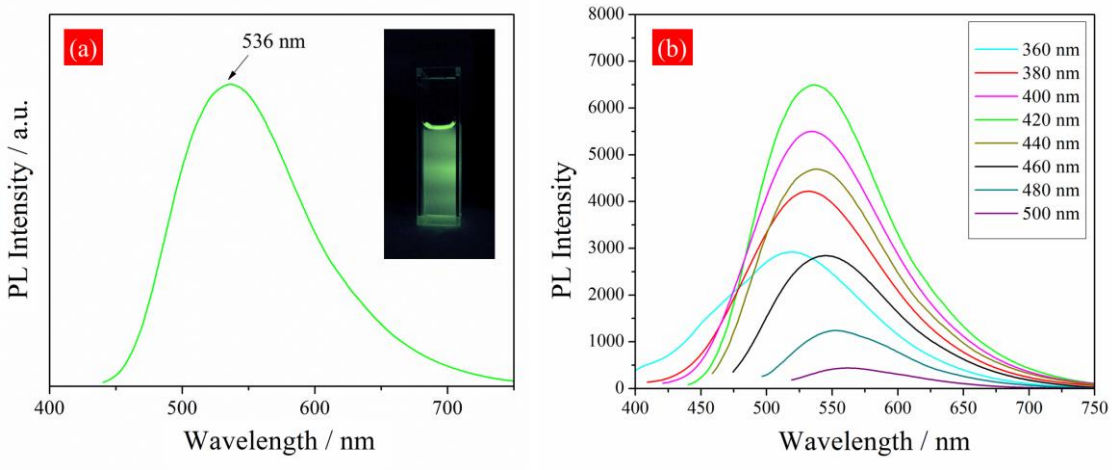

Figure 4.5. (a) PL emission spectrum (λ_{ex} = 420 nm) with a florescent digital image (inset) of CDs, and **(b)** PL spectra of the prepared CDs under different wavelengths of excitation.

The emission peak observed in the PL spectrum at 536 nm (excitation, λ_{ex} = 420 nm) represents the green colored fluorescence of the prepared CDs as shown in the digital image in the inset (**Figure 4.5(a)**). The presence of emissive traps has been previously reported to be the origin of the emission peak. These traps are formed due to the presence of functional group

related to surface states of CDs [18]. In addition, the excitation-dependent emissions of CDs were investigated under different excitation wavelengths (**Figure 4.5(b)**). The emission peak red-shifts to 550 nm (λ_{ex} = 500 nm) from 517 nm (λ_{ex} = 300 nm) with maximum intensity emission peak at 536 nm.

4.3.2.2 Optical properties of the dye and PGEs

To elucidate the optical behavior of the dye and the prepared PGEs, their UV-vis spectra were recorded. The N719 dye molecules exhibit maximum absorption (λ_{max}) at 533 nm in the visible region (**Figure 4.6(a)**). It also absorbs at 390 nm and 313 nm in the lower wavelength region. Consequently, the required λ_{max} for the absorption of CDs (~410 nm) is available for the DSSCs fabricated using N719 dye. The UV-vis absorption curves of the PGEs with varying amount of CDs reveal their optical properties (**Figure 4.6(b)**). The PGE without CDs (i.e., P(0)) absorbs light at 290 nm and 360 nm. This indicates that it does not absorb light responsible for the fluorescence of the CDs (~420 nm) as well as the light responsible for the dye excitation (~533 nm). Thus, the PGE based on PMMA is suitable as a gel electrolyte for DSSCs. With the addition of CDs in the PGEs, they exhibit an additional absorbance peak at around 410 nm. The intensity of the peak at this wavelength increases with the increase in the amount of CDs in the PGE upto 0.14 w/v %. Further addition of the CDs decreases the intensity of absorption due to agglomeration of the CDs as shown by the spectrum of PCD(0.17). This broadening of the absorbance range of the visible region for the prepared PGEs indicates that the electrolytes have potential to enhance the efficiency of the DSSC by converting more light to electrical energy.

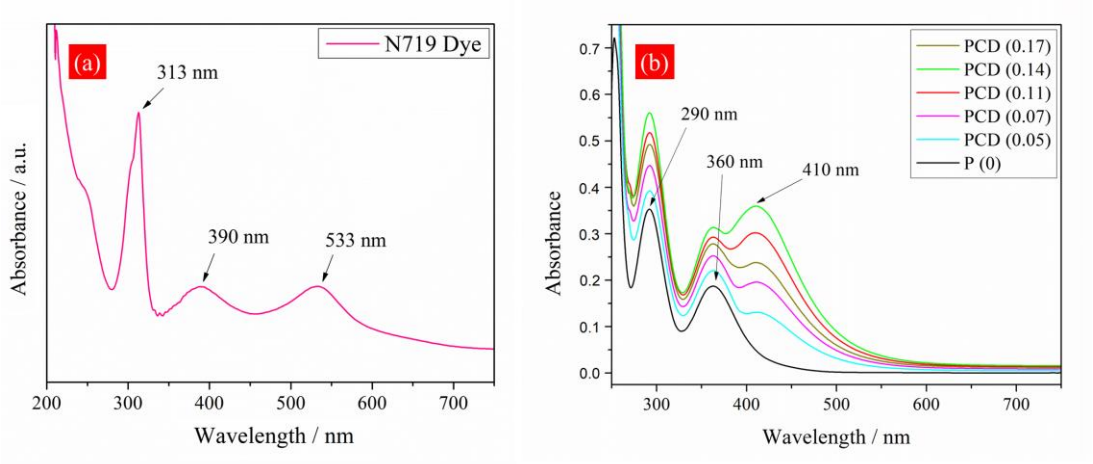

Figure 4.6. UV-vis spectra of **(a)** N719 dye and **(b)** PGEs with varying amount of CDs.

4.3.3 Photovoltaic performance of the DSSCs

To investigate the performance of the different PGEs, a series of DSSCs was fabricated and their photovoltaic parameters were recorded using *J-V* characteristic plots under solar illumination (**Figure 4.7**), and tabulated in **Table 4.1** [19].

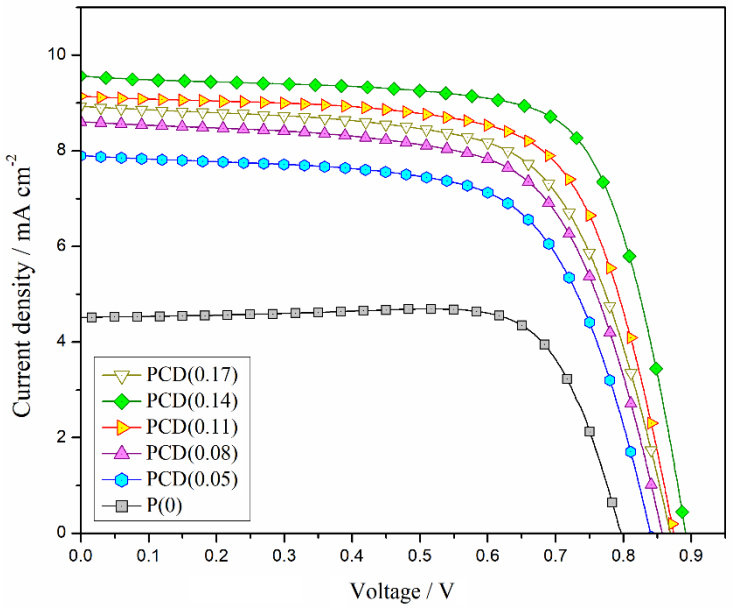

Figure 4.7. *J-V* characteristics of the fabricated DSSCs.

Table 4.1. Photovoltaic performances of the fabricated DSSCs.

Polymer gel electrolyte	J_{SC} / mA cm^{-2}	V_{OC} / V	***FF***	η / %
P(0)**	4.52	0.795	0.78	2.83
PCD(0.05)*	7.90	0.839	0.65	4.35
PCD(0.08)*	8.61	0.856	0.65	4.86
PCD(0.11)*	9.12	0.873	0.68	5.45
PCD(0.14)*	9.55	0.892	0.70	6.05
PCD(0.17)*	8.92	0.868	0.65	5.09

* PCD stands for PMMA/CD composite and the number within bracket represents the w/v % of added CD in the PMMA host.
** P stands for only PMMA (without CDs)

It is observed that all the photovoltaic parameters are improved with the addition of CDs and the highest photoconversion efficiency of 6.05% is exhibited by the optimized device fabricated using the electrolyte PCD(0.14) with short-circuit current density (J_{SC}) of 9.55 mA cm^{-2}, open-circuit voltage (V_{OC}) of 0.892 V and fill factor (FF) of 0.70. The cells show improvement in efficiency from 2.83% (without CDs) to 6.05% (with 0.14 w/v % CDs). Moreover, the V_{OC} value also jumps from 0.795 to 0.892 V and the J_{SC} value increases from 4.52 to 9.55 mA cm^{-2} for the DSSCs with electrolytes P(0) and PCD(0.14) respectively.

4.3.4 Enhancement of photovoltaic parameters

The magnitude of output voltage of DSSC is the difference in the potential between the quasi Fermi level of the TiO_2 semiconductor (E_F) and the redox potential of the iodide/triiodide (I^-/I_3^-) redox pair (E_{redox}) on irradiation of light [20]. This is mathematically represented as **Eq. (4.1)**.

$$V_{oc} = \frac{kT}{q}\left(\frac{E_c - E_{redox}}{kT} + \ln\frac{n_c}{N_c}\right) \quad \textbf{(4.1)}$$

where q, E_C, n_c and N_C are the charge, conduction band edge, free electron density and density of accessible state in the conduction band of TiO_2 respectively. k and T represent Boltzmann constant and temperature. The E_{redox} value for a specific redox pair is fixed. Consequently, the augmentation of V_{OC} is either due to higher E_c or higher n_C value in TiO_2. The value of E_C depends on the chemical capacitance ($C\mu$) developed at the interface between the electrolyte and photoanode.

To elucidate the effect of electrolyte on the E_C value, the capacitance values of different electrolytes were calculated under dark conditions by means of EIS (**Figure 4.8).** An applied bias of 0.80 V operates as the V_{OC} of the DSSC in dark condition. It is observed that the value of $C\mu$ remains constant for different PGEs at a given bias potential. It indicates that the enhancement of V_{OC} in the DSSCs does not depend upon the value of E_C, but only on the magnitude of n_c [21,22]. This improvement of V_{OC} in the presence of CDs can be better understood by using **Scheme 4.1. Scheme 4.1(a)** shows the various processes typically involved in the functioning of a DSSC, wherein only green light of the solar spectrum is converted into electrical energy. When CDs are incorporated in the system, they absorb unused higher energy light and emit green light (~533 nm) which can further excite electrons in the dye molecules form the valance band to the conduction band **(Scheme 4.1(b))**. This causes an increase in the conduction band electron density of the dye molecule. Subsequently, these electrons are transferred to the conduction band of TiO_2 causing further increase in n_c value and enhancement in the magnitude of the V_{OC} to

0.892 V from 0.795 V in the DSSC fabricated with PGE having green emitting fluorescent CDs and without having CDs respectively.

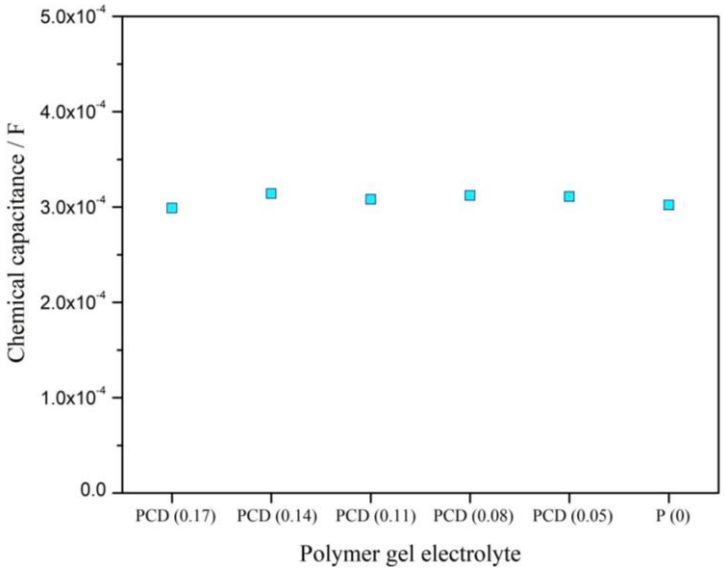

Figure 4.8. Chemical capacitance at the interface between the photoanode and different electrolytes.

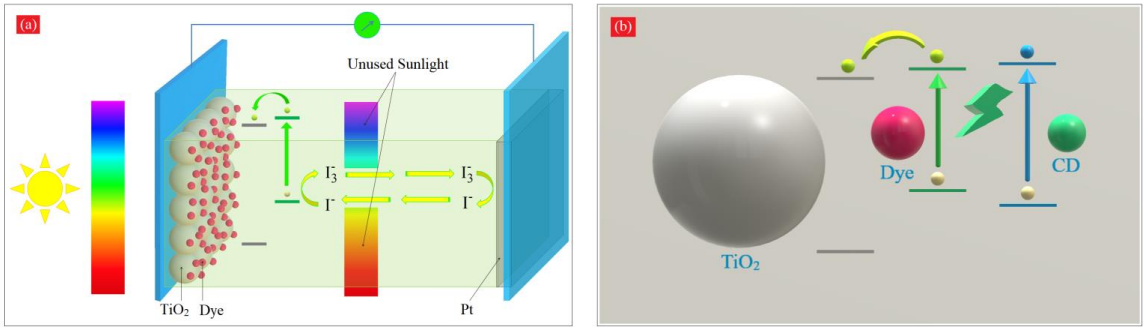

Scheme 4.1. Role of CDs in enhancing the photoconversion efficiency of DSSCs.

The *J-V* characteristics further demonstrate that the DSSCs employing PGEs with CDs show enhancement of J_{SC} values compared to the DSSC fabricated with PGE without CDs. The diffusion constant of the I_3^- ions together with the reaction rate of the redox pair determines the number of electron flow per unit time in the solar cell. A higher reduction rate and diffusion coefficient of I_3^- ions give higher J_{SC} value. In the presence of green emission from the CDs in PGE, more number of holes are generated in the valance band of the dye molecules, which in turn oxidizes more I^- ions to I_3^- ions. Subsequently, the rate of reduction of I_3^- ions increases at the Pt electrode, resulting in higher value of J_{SC}.

To quantify the reduction rate of I_3^- ions at the counter electrode, EIS measurements were carried out under irradiation of light (**Figure 4.9**).

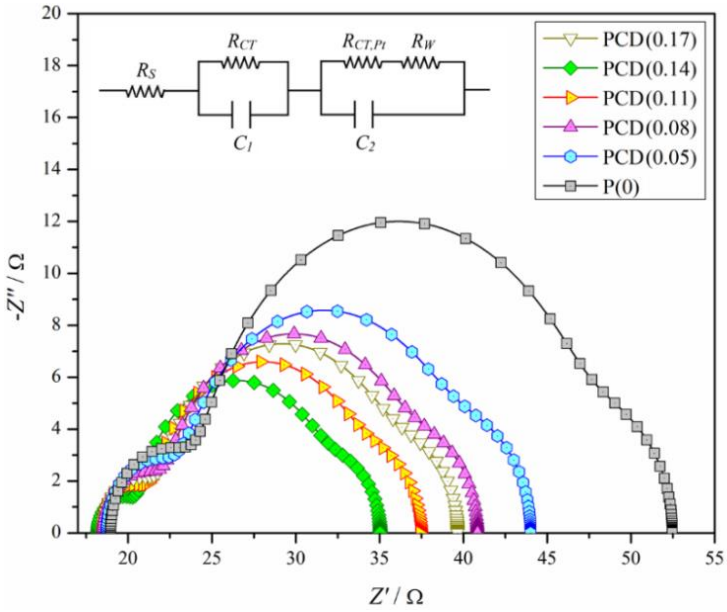

Figure 4.9. EIS plots of the DSSCs under irradiation of light.

Table 4.2. Electrochemical impedance and Tafel data of DSSCs fabricated with different PGEs.

Polymer gel electrolyte	$R_{CT,Pt}$ / Ω	R_{CT} / Ω	$D(\times 10^{-5})$ / cm^2 s^{-1}	$k_{I_3^-}$ / s^{-1}	J_{lim} / mA cm^{-2}
P(0)**	5.11	21.96	0.62	596.01	14.22
PCD(0.05)*	4.32	14.98	1.24	667.21	16.98
PCD(0.08)*	3.58	13.52	1.39	914.67	18.62
PCD(0.11)*	2.95	11.69	1.61	1256.81	21.37
PCD(0.14)*	2.28	10.44	1.78	2149.22	22.39
PCD(0.17)*	3.31	12.87	1.50	1057.47	19.95

* PCD stands for PMMA/CD composite and the number within bracket represents the w/v % of added CD in the PMMA host.

** P stands for only PMMA (without CDs).

The inset shows an equivalent circuit that was used to analyze the data [23,24]. Among the three semicircles, the one on the extreme left describes the processes involved at the interface of Pt electrode with the PGE, the middle one represents the processes involved at the photoanode/PGE interface, while the third arc expresses the diffusion of the I_3^- ions [25]. The reduction of I_3^- ions follows first order kinetics; thus the frequency obtained at the position of

maximum height of the first semicircle can be used to represent the rate constant ($k_{I_3^-}$) of the reduction reaction [26]. The calculated rate constants for different PGEs are presented in **Table 4.2**. The rate is highest (2149.22 s^{-1}) for the DSSC with PCD(0.14) indicating the highest J_{SC} value. Further addition of CDs in the gel matrix decreases the rate due to the agglomeration of the CDs. Additionally, to examine the diffusion of I_3^- ions, the diffusion coefficients of the I_3^- was computed from the recorded EIS data. Diffusion coefficients were calculated using the **Eq. (3.3)** described in Chapter 3.The calculated diffusion coefficient values of I_3^- ions are also presented in **Table 4.2**. The diffusion coefficient increases from 0.62×10^{-5} cm^2 s^{-1} to 1.78×10^{-5} cm^2 s^{-1} for DSSC without CDs and with 0.14 w/v% of CDs in the PGE respectively. This enhancement of the magnitude of the diffusion coefficient in the electrolyte contributes to a raise in in the magnitude of J_{SC} for the DSSCs fabricated with PGE with green emitting CDs.

The charge transfer resistances at the two different interfaces: photoanode/PGE (R_{CT}) and counter electrode/PGE ($R_{CT,Pt}$) are measured and tabulated in **Table 4.2**. Both these resistances decrease with the increment of the CDs in the PGEs. DSSC with PCD(0.14) exhibits the lowest R_{CT} and $R_{CT,Pt}$ values amongst other PGEs. According to Ohm's law at a fixed potential, current is high for low resistance. The decreases of the charge transfer resistances support the enhancement of the J_{SC} values found in the *J-V* characteristic plots.

Tafel plots were recorded from a potential range of -1 V to +1 V for quantifying the limiting current densities (J_{lim}) (**Figure 4.10**).

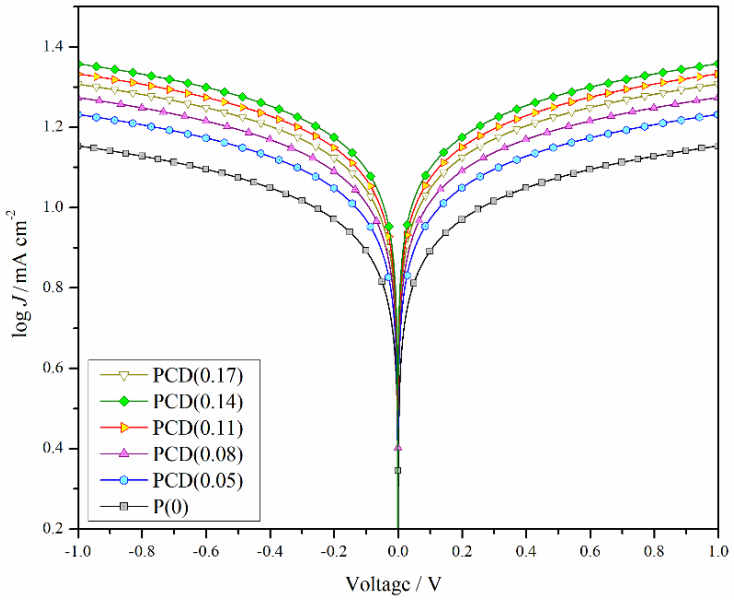

Figure 4.10. Tafel plots of the fabricated DSSCs.

The J_{lim} values obtained for the different DSSCs are also tabulated in **Table 4.2**, which show an increase in its value with the incorporation of CDs. The highest J_{lim} value obtained is

22.39 mA cm^{-1} (PCD(0.14)) while P(0) shows the lowest J_{lim} value of 14.22 mA cm^{-2} [27]. The recorded J_{lim} values of different DSSCs support the raise of the rates of electron transport processes at both the interfaces and the diffusion of I_3^- ions as observed from EIS parameters.

Incident photon-to-electron conversion efficiency (IPCE) is a powerful method that can be used to examine the photo-electrochemical behavior of the different DSSCs [28,29]. From the **Figure 4.11**, with the addition of CDs in the PGEs, a rise in the number of converted electrons is witnessed on exposure to photons. The rise of the IPCE onset is determined by two major factors: the number of photons absorbed by the cell and the number of electrons extracted from it. In the IPCE spectra, an additional peak at around 410 nm is observed in the PGEs with CDs. This broadening of the IPCE spectra is due to the additional absorption of photons with higher unexploited energy (~410 nm). Consequently, the raise and broadening of the IPCE in the PGEs with CDs enhances the efficiency of the DSSC. The IPCE of the DSSC with PCD(0.14) jumps to 70% from 50% (DSSC with P(0)). It is conclusive from the above studies that the CDs play a key role in enhancing IPCE by emitting green light while absorbing an additional part from the unexploited lower wavelengths of sunlight.

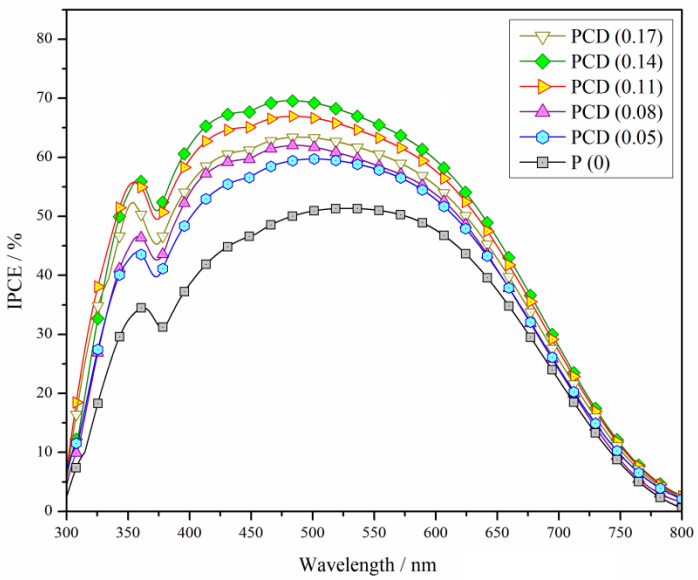

Figure 4.11. IPCE plots of the DSSCs.

J-V characteristics curves were recorded under dark conditions to examine the rate of electronic recombination at the interface of photoanode and different PGEs (**Figure 4.12**). From the values of current under dark conditions (**Figure 4.12(a)),** it is observed that PGE without CDs exhibits highest the dark current and among all the PGEs, while PGE with 0.14 w/v % of CDs shows the least dark current at a fixed potential. A higher value of dark current signifies higher recombination kinetics. Additionally, the influence of CDs in decreasing the

recombination kinetics is also supported by the open-circuit voltage decay (OCVD) studies with the fabricated devices. **Figure 4.12(b)** exhibits the change in V_{OC} as a function of time in the OCVD curves. From these plots, P(0) exhibits the fastest rate of V_{OC} decay indicating the highest recombination kinetics amongst all the prepared PGEs while PCD(0.14) shows the least voltage decay confirming the lowest recombination kinetics.

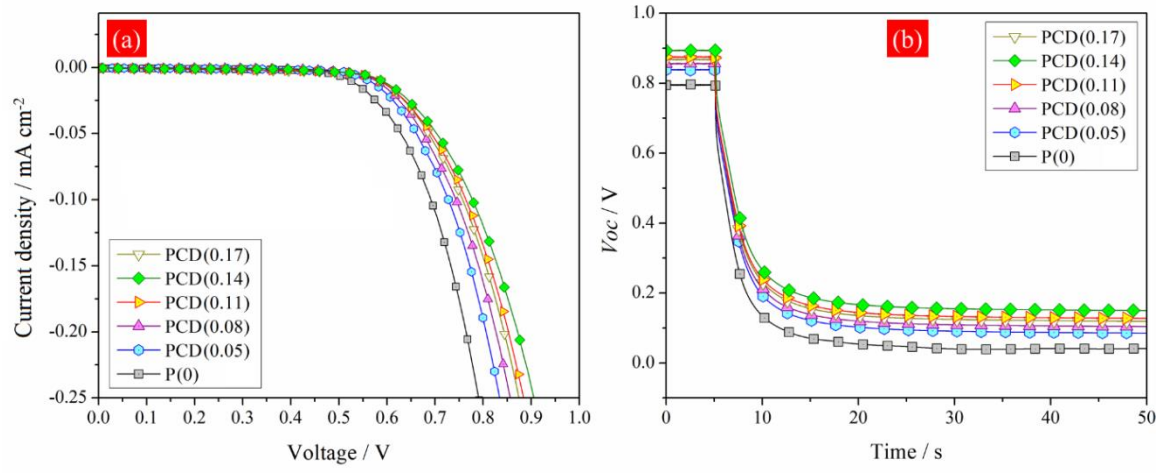

Figure 4.12. (a) *J-V* characteristics (dark conditions) and **(b)** OCVD profiles of different DSSCs.

4.3.5 Long-term stability analysis

Finally, to study the device's performance in the long run, the V_{OC} (**Figure 4.13(a)**) and J_{SC} (**Figure 4.13(b)**) values were recorded for upto 1000 h at 35 ºC [30]. All the DSSCs show significant stability. The V_{OC} values for all the devices remain similar after 1000 h of testing. However, small decrease in J_{SC} value is observed in every device. The J_{SC} values for DSSCs with PCD(0.17), PCD(0.14), PCD(0.11), PCD(0.08), PCD(0.05) and P(0) are retained at 88.1%, 96.7%, 96.4%, 95.9%, 97.2% and 96.4% of their initial performances.

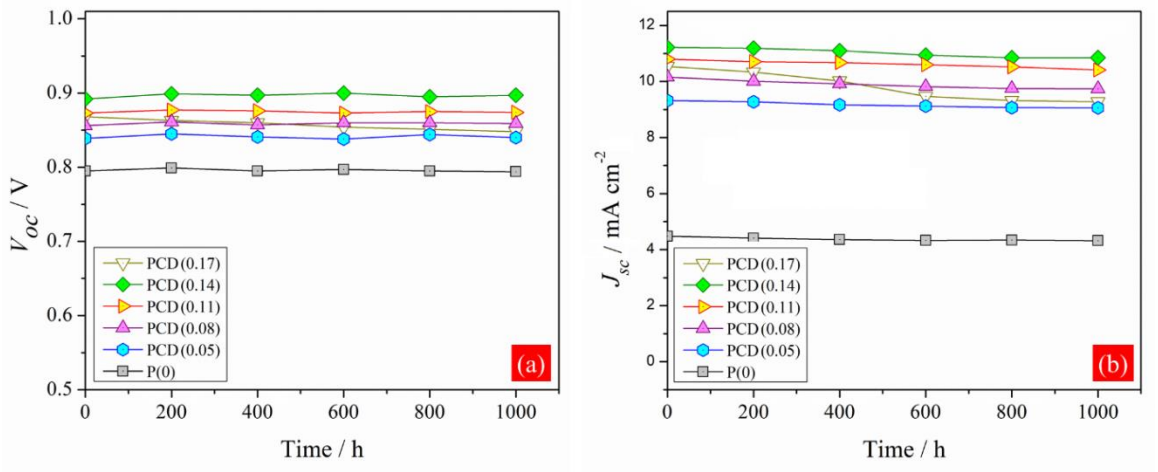

Figure 4.13. (a) V_{OC} and **(b)** J_{SC} values of the different DSSCs during 1000 h of testing.

PMMA contains a number of functional groups that hold the volatile organic electrolytes inside its matrix. Consequently, the PGE based DSSCs demonstrate significant durability without compromising its efficiency by overcoming the issues related to the leakage and evaporation of solvents.

4.4 Conclusion

- A stable and highly efficient quasi-solid-state DSSC was fabricated using PMMA and carbon dots based PGE.
- Optical analyses of the PGEs showed that the PGEs with CDs broadened the sunlight absorption range of the device.
- The optimized quasi-solid-state cell fabricated using 0.14 w/v% CDs showed a photoconversion efficiency of 6.05% with V_{OC} value of 0.892 V and J_{SC} value of 9.55 mA cm^{-2} under illumination of 100 mW cm^{-2} (AM 1.5) light.
- The enhancement of the photoconversion efficiency on addition of CDs was due to the broadening of the range of sunlight absorbed by the cell in presence of the green emitting CDs in the PGE. This was also evident in the incident photon-to-electron efficiency plots. The green light emitted from the CDs created additional photoexcited electrons and increased their density at the conduction band of the semiconductor.
- The DSSC with 0.14 w/v% CDs exhibited a significant long-term stability with 96.7% retention of the initial J_{SC} value (at 35^{o}C) after 1000 h of testing.

4.5 References

[1] Yun, H. J., Jung, D. Y., Lee, D. K., Jen, A. K. Y., and Kim, J. H. Panchromatic quasi-solid-state squaraine dye sensitized solar cells enhanced by Förster resonance energy transfer of DCM-pyran. *Dyes and Pigments*, 113:675-681, 2015.

[2] Yao, N., Huang, J., Fu, K., Deng, X., Ding, M., and Xu, X. Rare earth ion doped phosphors for dye-sensitized solar cells applications. *RSC Advances*, 6(21):17546-17559, 2016.

[3] Paulo, S., Palomares, E., and Martinez-Ferrero, E. Graphene and carbon quantum dot-based materials in photovoltaic devices: From synthesis to applications. *Nanomaterials*, 6(9):157, 2016.

[4] Huang, J. J., Zhong, Z. F., Rong, M. Z., Zhou, X., Chen, X. D., and Zhang, M. Q. An easy approach of preparing strongly luminescent carbon dots and their polymer based composites for enhancing solar cell efficiency. *Carbon*, 70:190-198, 2014.

[5] Zhu, S., Meng, Q., Wang, L., Zhang, J., Song, Y., Jin, H., Zhang, K., Sun, H., Wang, H., and Yang, B. Highly photoluminescent carbon dots for multicolor patterning, sensors, and bioimaging. *Angewandte Chemie - International Edition*, 52(14):3953-3957, 2013.

[6] Wang, H., Sun, C., Chen, X., Zhang, Y., Colvin, V. L., Rice, Q., Seo, J., Feng, S., Wang, S., and William, W. Y. Excitation wavelength independent visible color emission of carbon dots. *Nanoscale*, 9(5):1909-1915, 2017.

[7] Wu, J., Lan, Z., Lin, J., Huang, M., Huang, Y., Fan, L., and Luo, G. Electrolytes in dye-sensitized solar cells. *Chemical Reviews*, 115(5):2136-2173, 2015.

[8] Zheng, J. Graphene tailored polymer gel electrolytes for 9.1%-efficiency quasi-solid-state dye-sensitized solar cells. *Journal of Power Sources*, 348:239-245, 2017.

[9] Sonai, G. G., Tiihonen, A., Miettunen, K., Lund, P. D., and Nogueira, A. F. Long-term stability of dye-sensitized solar cells assembled with cobalt polymer gel electrolyte. *The Journal of Physical Chemistry C*, 121(33):acs.jpcc.7b03865, 2017.

[10] Su'ait, M. S., Rahman, M. Y. A., and Ahmad, A. Review on polymer electrolyte in dye-sensitized solar cells (DSSCs). *Solar Energy*, 115:452-470, 2015.

[11] Khan, W. U., Wang, D., Zhang, W., Tang, Z., Ma, X., Ding, X., Du, S., and Wang, Y. High quantum yield green-emitting carbon dots for Fe(III) detection, biocompatible fluorescent ink and cellular imaging. *Scientific Reports*, 7(1):14866, 2017.

[12] Mohan, K., Dolui, S., Nath, B. C., Bora, A., Sharma, S., and Dolui, S. K. A highly stable and efficient quasi solid state dye sensitized solar cell based on polymethyl methacrylate (PMMA)/carbon black (CB) polymer gel electrolyte with improved open circuit voltage. *Electrochimica Acta*, 247:216-228, 2017.

[13] Mohan, K., Bora, A., Nath, B. C., Gogoi, P., Saikia, B. J., and Dolui, S. K. A highly stable and efficient quasi solid state dye sensitized solar cell based on polymethyl methacrylate(PMMA)/polyaniline nanotube(PANI-NT) gel electrolyte. *Electrochimica Acta*, 222:1072-1078, 2016.

[14] Li, Q., Wu, J., Tang, Z., Xiao, Y., Huang, M., and Lin, J. Application of poly(acrylic acid-g-gelatin)/polypyrrole gel electrolyte in flexible quasi-solid-state dye-sensitized solar cell. *Electrochimica Acta*, 55(8):2777-2781, 2010.

[15] Lin, L. Y., Tsai, C. H., Wong, K. T., Huang, T. W., Hsieh, L., Liu, S. H., Lin, H. W., Wu, C. C., Chou, S. H., Chen, S. H., and Tsai, A. I. Organic dyes containing coplanar diphenyl-substituted dithienosilole core for efficient dye-sensitized solar cells. *Journal of Organic Chemistry*, 75(14):4778-4785, 2010.

[16] Chen, B. B., Liu, Z. X., Deng, W. C., Zhan, L., Liu, M. L., and Huang, C. Z. A large-scale synthesis of photoluminescent carbon quantum dots: A self-exothermic reaction driving the formation of the nanocrystalline core at room temperature. *Green Chemistry*, 18(19):5127-5132, 2016.

[17] Xu, M., He, G., Li, Z., He, F., Gao, F., Su, Y., Zhang, L., Yang, Z., and Zhang, Y. A green heterogeneous synthesis of N-doped carbon dots and their photoluminescence applications in solid and aqueous states. *Nanoscale*, 6(17):10307-10315, 2014.

[18] Tang, L., Ji, R., Cao, X., Lin, J., Jiang, H., Li, X., Teng, K. S., Luk, C. M., Zeng, S., Hao, J., and Lau, S. P. Deep ultraviolet photoluminescence of water-soluble self-passivated graphene quantum dots. *ACS Nano*, 6(6):5102-5110, 2012.

[19] Yu, J., Fan, J., and Lv, K. Anatase TiO_2 nanosheets with exposed (001) facets: Improved photoelectric conversion efficiency in dye-sensitized solar cells. *Nanoscale*, 2(10):2144-2149, 2010.

[20] Wu, C., Jia, L., Guo, S., Han, S., Chi, B., Pu, J., and Jian, L. Open-circuit voltage enhancement on the basis of polymer gel electrolyte for a highly stable dye-sensitized solar cell. *ACS applied materials & interfaces*, 5(16):7886-7892, 2013.

[21] Barea, E. M., Ortiz, J., Payá, F. J., Fernández-Lázaro, F., Fabregat-Santiago, F., Sastre-Santos, A., and Bisquert, J. Energetic factors governing injection, regeneration and recombination in dye solar cells with phthalocyanine sensitizers. *Energy and Environmental Science*, 3(12):1985-1994, 2010.

[22] Bisquert, J. Chemical capacitance of nanostructured semiconductors: Its origin and significance for nanocomposite solar cells. *Physical Chemistry Chemical Physics*, 5(24):5360-5364, 2003.

[23] Bisquert, J. Theory of the impedance of electron diffusion and recombination in a thin

layer. *Journal of Physical Chemistry B*, 106(2):325-333, 2002.

[24] Bisquert, J., Grätzel, M., Wang, Q., and Fabregat-Santiago, F. Three-channel transmission line impedance model for mesoscopic oxide electrodes functionalized with a conductive coating. *Journal of Physical Chemistry B*, 110(23):11284-11290, 2006.

[25] Yue, G., Ma, X., Zhang, W., Li, F., Wu, J., and Li, G. A highly efficient flexible dye-sensitized solar cell based on nickel sulfide/platinum/titanium counter electrode. *Nanoscale Research Letters*, 10(1):1-9, 2015.

[26] Adachi, M., Sakamoto, M., Jiu, J., Ogata, Y., and Isoda, S. Determination of parameters of electron transport in dye-sensitized solar cells using electrochemical impedance spectroscopy. *Journal of Physical Chemistry B*, 110(28):13872-13880, 2006.

[27] Bard, A. J. and Faulkner, L. R. *Electrochemical methods : Fundamentals and applications*. Wiley, New York, 2nd edition, 2001.

[28] Ren, Y. K., Ding, X. H., Wu, Y. H., Zhu, J., Hayat, T., Alsaedi, A., Xu, Y. F., Li, Z. Q., Yang, S. F., and Dai, S. Y. Temperature-assisted rapid nucleation: A facile method to optimize the film morphology for perovskite solar cells. *Journal of Materials Chemistry A*, 5(38):20327-20333, 2017.

[29] He, Z., Hou, Z., Xing, Y., Liu, X., Yin, X., Que, M., Shao, J., Que, W., and Stang, P. J. Enhanced conversion efficiencies in dye-sensitized solar cells achieved through self-assembled platinum(II) metallacages. *Scientific Reports*, 6:29476, 2016.

[30] Jung, H., Koo, B., Kim, J. Y., Kim, T., Son, H. J., Kim, B., Kim, J. Y., Lee, D. K., Kim, H., Cho, J., and Ko, M. J. Enhanced photovoltaic properties and long-term stability in plasmonic dye-sensitized solar cells via noncorrosive redox mediator. *ACS Applied Materials and Interfaces*, 6(21):19191-19200, 2014.